Gas-phase CO2, C2H2 and HCN toward Orion-KL

Boonman, A.M.S.; Dishoeck, E.F. van; Lahuis, F.; Doty, S.D.; Wright, C.M.; Rosenthal, D.

Astronomy
&
Astrophysics

Gas-phase CO$_2$, C$_2$H$_2$, and HCN toward Orion-KL[*]

A. M. S. Boonman[1], E. F. van Dishoeck[1], F. Lahuis[1,2], S. D. Doty[3], C. M. Wright[4], and D. Rosenthal[5]

[1] Sterrewacht Leiden, PO Box 9513, 2300 RA Leiden, The Netherlands
[2] SRON National Institute for Space Research, PO Box 800, 9700 AV Groningen, The Netherlands
[3] Department of Physics and Astronomy, Denison University, Granville, Ohio 43023, USA
[4] School of Physics, University College, ADFA, UNSW, Canberra ACT 2600, Australia
[5] Max-Planck-Institut für Extraterrestrische Physik, Giessenbachstrasse, 85741 Garching, Germany

Abstract. The infrared spectra toward Orion-IRc2, Peak 1 and Peak 2 in the 13.5–15.5 μm wavelength range are presented, obtained with the Short Wavelength Spectrometer on board the Infrared Space Observatory. The spectra show absorption and emission features of the vibration-rotation bands of gas-phase CO$_2$, HCN, and C$_2$H$_2$, respectively. Toward the deeply embedded massive young stellar object IRc2 all three bands appear in absorption, while toward the shocked region Peak 2 CO$_2$, HCN, and C$_2$H$_2$ are seen in emission. Toward Peak 1 only CO$_2$ has been detected in emission. Analysis of these bands shows that the absorption features toward IRc2 are characterized by excitation temperatures of ~175–275 K, which can be explained by an origin in the shocked plateau gas. HCN and C$_2$H$_2$ are only seen in absorption in the direction of IRc2, whereas the CO$_2$ absorption is probably more widespread. The CO$_2$ emission toward Peak 1 and 2 is best explained with excitation by infrared radiation from dust mixed with the gas in the warm component of the shock. The similarity of the CO$_2$ emission and absorption line shapes toward IRc2, Peak 1 and Peak 2 suggests that the CO$_2$ is located in the warm component of the shock ($T \sim 200$ K) toward all three positions. The CO$_2$ abundances of ~10^{-8} for Peak 1 and 2, and of a few times 10^{-7} toward IRc2 can be explained by grain mantle evaporation and/or reformation in the gas-phase after destruction by the shock. The HCN and C$_2$H$_2$ emission detected toward Peak 2 is narrower ($T \sim 50$–150 K) and originates either in the warm component of the shock or in the extended ridge. In the case of an origin in the warm component of the shock, the low HCN and C$_2$H$_2$ abundances of ~10^{-9} suggest that they are destroyed by the shock or have only been in the warm gas for a short time ($t \lesssim 10^4$ yr). In the case of an origin in the extended ridge, the inferred abundances are much higher and do not agree with predictions from current chemical models at low temperatures.

Key words. stars: formation – ISM: individual objects: Orion IRc2, Peak 1, Peak 2 – ISM: abundances – ISM: molecules – ISM: lines and bands – molecular processes

1. Introduction

The Orion-IRc2/KL region ($d \approx 450$ pc) has traditionally been the prime source for studies in astrochemistry because of its extraordinarily rich spectra. Millimeter and submillimeter single-dish surveys show thousands of lines of nearly a hundred different molecules (e.g., Blake et al. 1987; Sutton et al. 1995; Schilke et al. 1997, 2001), whereas interferometer studies reveal intriguing chemical differentiation over scales of less than 2000 AU (e.g., Wright et al. 1996; Blake et al. 1996). In spite of this wealth of data, molecules such as CO$_2$ and C$_2$H$_2$, which are symmetric and thus lack a dipole moment, cannot be observed through rotational transitions at millimeter

wavelengths. Moreover, CO$_2$ cannot be observed from Earth due to its high abundance in our atmosphere. Evans et al. (1991) have shown that important complimentary information can be obtained from vibration-rotation absorption lines toward bright mid-infrared sources. We present here spectra in the 13.5–15.5 μm range toward three positions in the core of the Orion molecular cloud, taken with the Short Wavelength Spectrometer (SWS) on board the *Infrared Space Observatory* (ISO), which are unhindered by the Earth's atmosphere. Absorption and emission features of CO$_2$, C$_2$H$_2$ and HCN are detected, which can be used to constrain the physical structure of this complex region and study the different chemistry of these molecules.

Millimeter studies have revealed a number of different physical and kinematic components in a 30″ region around the infrared source IRc2 (see Genzel & Stutzki 1989 for an overview). A clumpy hot core is located immediately adjacent to IRc2, with the clump exteriors currently being

---

evaporated and/or ablated by the winds from the embedded massive young stellar object(s) (YSOs). This hot core is contained in a cavity, surrounded by a torus of dense, quiescent gas (the extended ridge) in the NE-SW direction. To the NW and SE, two shocked regions – called Peak 1 and Peak 2 – are revealed by bright H_2 2 μm emission, indicating the positions where the high-velocity plateau or outflow runs into the ambient molecular cloud. Peak 1 is located ~25″ NW and Peak 2 ~ 24″ SE of IRc2 (Beckwith et al. 1978). A cartoon of the core of the Orion molecular cloud indicating these different physical components is shown in Fig. 1.

The ISO-SWS beam ranges from 14″ × 20″ to 20″ × 27″, so that these different regions can be separated spatially with the SWS. The 2.4–45.2 μm ISO-SWS spectrum toward IRc2 has been presented by van Dishoeck et al. (1998) and shows many features including emission lines of ionized species, PAHs, H_2, as well as absorption by interstellar ices and gas-phase species (see also Wright et al. 2000; González-Alfonso et al. 1998; Harwit et al. 1998). The full SWS spectrum toward Peak 1 has been presented by Rosenthal et al. (2000), whilst that toward Peak 2 is broadly similar (Wright 2000 and priv. comm. 2002). González-Alfonso et al. (1998) discuss the CO and H_2O vibrational emission bands toward Peak 1 and 2. Because of the weaker continuum, the lines are more prominent at these positions than toward IRc2, especially the vibration-rotation and pure-rotational lines of H_2.

In this paper, we focus on the ro-vibrational bands of gas-phase CO_2, C_2H_2, and HCN along the lines of sight toward IRc2, Peak 1 and Peak 2. CO_2 is predicted to be one of the more abundant carbon- and oxygen-bearing species and is detected ubiquitously in interstellar ices, with abundances of ~15% with respect to H_2O ice, or ~10^{-5}–10^{-6} with respect to H_2 (e.g. Gerakines et al. 1999). In contrast, the gas-phase CO_2 abundance is surprisingly low, ~10^{-7}, toward massive YSOs (van Dishoeck et al. 1996; van Dishoeck 1998; Dartois et al. 1998; Boonman et al. 2000). Since the abundances of many gas-phase species are enhanced toward IRc2, in particular those of species involved in the gas-grain chemistry (e.g., Blake et al. 1987; Charnley et al. 1992), it is important to investigate whether the CO_2 chemistry follows this trend. Observations of C_2H_2 and HCN are interesting because they are both significant in the carbon- and nitrogen chemistry, and because their excitation provides information on the physical conditions (Lahuis & van Dishoeck 2000). For HCN, rotational transitions in the sub-millimeter and ro-vibrational transitions in the infrared can be observed. In a number of massive YSOs the HCN abundance derived from submillimeter observations is a factor of ~100 lower than that derived from infrared observations, suggesting a jump in its abundance in high temperature regions (Lahuis & van Dishoeck 2000; van der Tak et al. 1999, 2000; Boonman et al. 2001). There is still considerable debate whether such abundance jumps are mainly due to evaporation of ices, to quiescent high-temperature chemistry at a few hundred K or to shock chemistry at a few thousand K. The comparison of the Orion IRc2 and the shocked Peak 1 and Peak 2 results can provide constraints on the different models.

In Sect. 2, the ISO-SWS data reduction methods are discussed. Section 3 will present models for the HCN, C_2H_2,
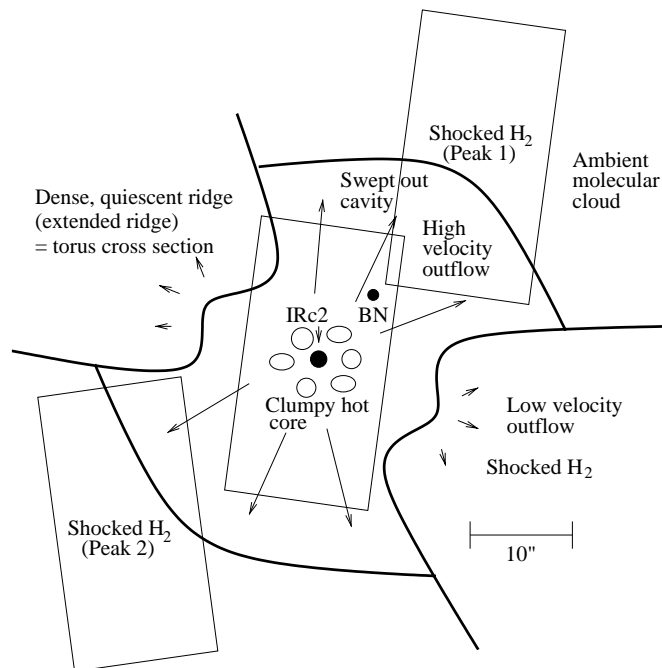

Fig. 1. Cartoon of the core of the Orion molecular cloud. The figure represents a cross section in the plane of the sky. The size and orientation of the ISO-SWS beam around 15 μm at the approximate positions of IRc2, Peak 1 and Peak 2 are indicated by the rectangular boxes (adapted from van Dishoeck et al. 1998).

and CO_2 absorption toward Orion IRc2. The inferred abundances are compared with those found toward other sources. In Sect. 4, the observations toward the shock positions Peak 1 and 2 are presented, and the excitation of the molecules is analyzed. Section 5 will compare the results for the three different positions and the conclusions are presented in Sect. 6.

2. Observations and reduction

The spectra toward Orion IRc2, Peak 1 and Peak 2 from 12.0–16.5 μm were made with the ISO-SWS grating. IRc2 was observed on September 6 1997 (revolution 660) using the SWS06 observing mode centered at $\alpha(1950) = 05^h32^m46.8^s$, $\delta(1950) = -05°24'25''$, which is about 1″ S and 3″ W of the IRc2 position listed by Gezari (1992). The Peak 1 spectrum was taken at the position $\alpha(1950) = 05^h32^m46.3^s$, $\delta(1950) = -05°24'2''$ in the SWS01 speed 4 observing mode, on October 3, 1997 (revolution 687). Finally, on February 25 1998 (revolution 833) the spectrum toward Peak 2 was taken using the SWS01 speed 4 observing mode at the position $\alpha(1950) = 05^h32^m48.4^s$, $\delta(1950) = -05°24'34''$, ~1″ E of the position listed by Beckwith et al. (1978). The beam size in this wavelength range is 14″ × 27″, and was oriented ~7° and ~11° in NW-SE direction for IRc2 and Peak 2 respectively. These two beams do not overlap; however, the infrared source BN falls within the IRc2 beam (see sketch of region in Fig. 1). The Peak 1 beam, which has the same size and is orientated ~6° in NE-SW direction, partially overlaps with the IRc2 beam, but does not contain the BN object at the observed wavelength range.
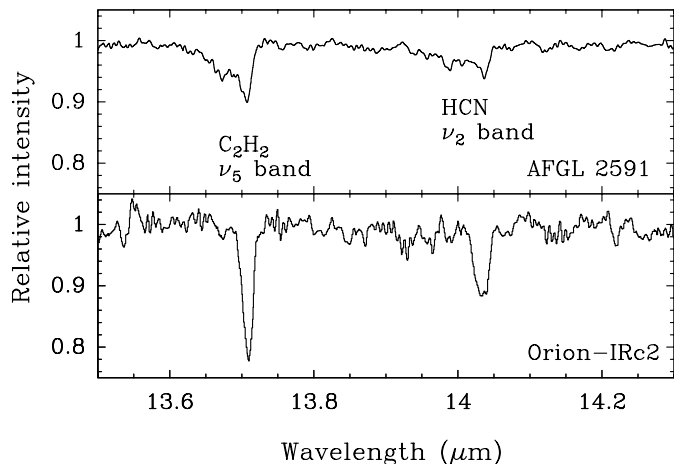
Fig. 2. Comparison of the 13.5–14.3 μm spectra toward the massive young stellar objects Orion-IRc2 and AFGL 2591. The HCN and C_2H_2 Q-branches toward Orion-IRc2 are much narrower than those toward AFGL 2591, and the absence of the hot bands at 13.7 and 14.0 μm indicates that less warm gas is probed ($T_{ex} < 400$ K). The AFGL 2591 spectrum is adapted from Lahuis & van Dishoeck (2000).

Table 1. Model parameters for the absorption toward Orion-IRc2[a].

Molecule	T_{ex}	N	b
	(K)	(10^{16} cm^{-2})	(km s^{-1})
HCN[b]	275^{+40}_{-55}	$5.0^{+2.8}_{-1.7}$	3
HCN[b]	275^{+55}_{-55}	$4.5^{+2.0}_{-1.7}$	5
HCN[b]	300^{+50}_{-75}	$4.2^{+2.0}_{-1.4}$	10
C_2H_2[b]	160^{+40}_{-40}	$2.5^{+1.4}_{-1.0}$	3
C_2H_2[b]	175^{+50}_{-50}	$1.9^{+0.9}_{-0.6}$	5
C_2H_2[b]	175^{+50}_{-50}	$1.6^{+0.7}_{-0.5}$	10
CO_2[b]	120^{+70}_{-30}	100^{+700}_{-65}	3
CO_2[b]	180^{+60}_{-60}	26^{+34}_{-11}	5
CO_2[b]	200^{+60}_{-60}	16^{+8}_{-6}	10
CO_2	220^{+40}_{-40}	$6.5^{+0.6}_{-0.6}$	3
CO_2	220^{+40}_{-40}	$5.0^{+0.6}_{-0.3}$	5
CO_2	250^{+25}_{-40}	$5.0^{+0.2}_{-0.2}$	10

[a] Filling in by emission has not been included, but it is only important for HCN. For CO_2 and C_2H_2 the effect is $\lesssim 25\%$, which is within the error bars (see text).

[b] With 62% BN continuum subtracted (see text).

Data reduction was done within the ISO-SWS Interactive Analysis System SIA using the ISO Off-line Processing (OLP version 10) software modules and calibration files (see Lahuis et al. 1998 and Wieprecht et al. 2001 for a description of the SIA system and its relation to the ISO OLP system). For the SWS01 observations the Standard Processed Data (SPD) were re-derived to create spectra at full grating resolution with some loss in signal to noise. This software has been developed at the Dutch ISO Data Analysis Centre (DIDAC) and is based on the OLP software and calibration. It will become available within SIA and OSIA[1] for general use. Instrumental fringes have been minimized when applying the Instrumental Spectral Response Function (RSRF) by RSRF matching to allow for offsets in the wavelength calibration and differences in resolution between the data and the RSRF. The remaining fringe residuals after the RSRF calibration were removed using a robust iterative sine fitting method based on an approximated Fabry-Pérot model (see Lahuis & van Dishoeck 2000 and Kester et al. 2001). All spectra have been rebinned to a spectral resolving power of 3500, twice the instrumental resolution. The final spectra have a typical S/N ratio on the continuum of 50–100.

3. Molecular absorption toward IRc2

3.1. HCN and C_2H_2

The ISO-SWS spectrum of the ν_5 ro-vibrational band of gas-phase C_2H_2 at 13.71 μm and the ν_2 ro-vibrational band of gas-phase HCN at 14.05 μm toward IRc2 are presented in Fig. 2. The strong Q-branch features of both species are clearly detected in absorption. They are much narrower than the HCN and C_2H_2 Q-branch features detected toward massive protostars, such as AFGL 2591 and AFGL 2136

[1] The Observers SWS Interactive Analysis (OSIA) package can be downloaded from http://sws.ster.kuleuven.ac.be/. It is a package for SWS processing using IDL.

(Lahuis & van Dishoeck 2000), indicating lower excitation temperatures (see Fig. 2). The HCN and C_2H_2 hot bands at 14.00 μm and 14.30 μm for HCN, and 13.72 μm and 13.89 μm for C_2H_2, seen toward the latter sources are not detected toward IRc2, implying that the excitation temperature of the observed HCN and C_2H_2 gas is <400 K.

No R- or P-branch lines have been detected for HCN and C_2H_2. Some R-branch lines at 13.5 μm of HCN and C_2H_2 were previously observed from the ground by Evans et al. (1991) at higher resolving power, $\lambda/\Delta\lambda \approx 15\,000$. Their observations were made with a $\sim 3'' \times 3''$ beam, which is much smaller than the ISO-SWS beam, allowing IRc2 and BN to be observed separately. A disadvantage of these ground-based data is the need to correct for atmospheric transmission. Since no HCN and C_2H_2 absorption was detected toward BN, Evans et al. (1991) divided their IRc2 spectra by the BN spectra to remove the telluric features. The much stronger Q−branch features seen in the ISO-SWS spectra are difficult to observe from Earth due to telluric interference.

Based on the Evans et al. (1991) data, it is likely that the absorption occurs only toward the area directly surrounding IRc2. This area includes the infrared sources IRc2, IRc7, and IRc4, which are the dominant sources between 12 and 20 μm (Gezari et al. 1992). However, Evans et al. (1991) show that most of the absorbing C_2H_2 gas lies in front of IRc2 and IRc7 and that the HCN and C_2H_2 column densities toward IRc2 are a factor of $\gtrsim 2$ higher than toward IRc7. Therefore, we assume in our analysis that the absorption occurs only toward IRc2, although some contribution from the line of sight toward IRc7 may be present. The fraction of the continuum flux due to BN at 13.5 μm in the ISO-SWS beam has been estimated to be $\sim 62 \pm 6\%$ from

mid-infrared maps by Downes et al. (1981) and Wynn-Williams et al. (1984) and is corrected for the beam profile by comparing our ISO-SWS spectrum centered at IRc2 with that centered at BN (Cernicharo et al., unpublished results). The BN continuum flux has been subtracted from the total flux in the ISO-SWS beam, resulting in a spectrum in which the absorption lines are superposed on the IRc2 continuum only. This spectrum has then been divided by the IRc2 continuum to get the relative absorption spectrum. The percentage of BN continuum has been varied from 55% to 68% and the corresponding values have been included as error bars in Table 1.

The normalized spectra have been analyzed using synthetic absorption spectra as described by Lahuis & van Dishoeck (2000). These model fits depend only on the excitation temperature T_{ex}, the total column density of the molecule N and the Doppler broadening parameter b. Because of the high densities in Orion, the C_2H_2 and HCN excitation is likely to be close to thermal, and can be described by a single excitation temperature. Recently, new high-resolution ground-based observations of IRc2 around 13.3 μm with the Texas Echelon-Cross-Echelle Spectrograph (TEXES) have been performed at a spectral resolving power of $\lambda/\Delta\lambda \sim 100\,000$ (Lacy et al. 2002). In these spectra the individual R-branch lines of C_2H_2 and HCN are resolved and have a range of Doppler b parameters of $\sim$3–10 km s^{-1} (Lacy, priv. comm), compared to $b \sim$3 km s^{-1} found by Carr et al. (1995). Therefore different b-values between 3 and 10 km s^{-1} have been explored in the models. Because of the low spectral resolution of the ISO-SWS, the absorption seen in our spectra is expected to be dominated by the components with the larger line widths.

The best fit model for C_2H_2 has an excitation temperature of $T_{ex} = 175$ K and a column density of $N = 1.9 \times 10^{16}$ cm^{-2}, whereas that for HCN has $T_{ex} = 275$ K and $N = 4.5 \times 10^{16}$ cm^{-2}. These values are listed in Table 1 along with the error bars obtained from χ^2_ν fits. The C_2H_2 excitation temperature corresponds well with values derived by Carr et al. (1995), who re-analyzed the data from Evans et al. (1991). The HCN excitation temperature corresponds well to the $T \sim 300$ K derived for the hot core (Blake et al. 1987; Wright et al. 1996), but not with that of $\sim$132 K listed in Carr et al. (1995). Based on kinematic grounds combined with their excitation temperatures, Evans et al. (1991) concluded that the HCN and C_2H_2 absorption probably originates in the plateau gas. However the HCN excitation temperature found here is higher than their value. This may be partly due to the fact that the lower spectral resolution ISO-SWS data are less sensitive to the colder, less turbulent gas, with small line widths. In addition, a high-resolution map of H^{13}CN toward IRc2 by Wright et al. (1996) reveals the presence of several clumps with temperatures $\gtrsim$150 K. These warm clumps fall outside the $\sim$3″ beam used by Evans et al. (1991), but within the ISO-SWS beam. If these clumps are in front of an infrared source, this probably explains the higher HCN excitation temperature derived from the ISO-SWS spectra. Higher-resolution spectra such as those by Lacy et al. (2002, in prep.) can help to disentangle the different components present along the line of sight.

It should be noted that a significant fraction of cold HCN and C_2H_2 gas could still be hidden in the low-resolution ISO-SWS spectra, which is picked up in higher-resolution ground-based spectra (Evans et al. 1991; Lacy et al. 2002, in prep.). This could explain why both the HCN and C_2H_2 column densities are a factor of 4–5 lower than the values N(HCN) $= 1.8 \times 10^{17}$ cm^{-2} and N(C_2H_2) $= 0.95 \times 10^{17}$ cm^{-2} previously derived by Carr et al. (1995).

The models used so far assume pure absorption and do not include possible emission in the line itself. In order to examine its effect on the derived column density, an excitation model has been set-up including levels up to $J = 21$ in the ground and $\nu_2 = 1$ vibrational states for HCN and up to $J = 24$ for C_2H_2. A blackbody with $T \sim 300$ K has been adopted as background source, corresponding to the temperature found by Gezari et al. (1998) for IRc2. Excitation temperatures ranging from 125 to 175 K for C_2H_2 and 220 to 330 K for HCN have been explored, corresponding to the values listed in Table 1, assuming that the populations in both the $\nu_2 = 0$ and $\nu_2 = 1$ state follow a Boltzmann distribution at these temperatures. For C_2H_2 the derived column densities are $\sim$25% higher if emission in the line is included, which is not significant. Because of the higher excitation temperatures, this effect does play a role for HCN, where it becomes important whenever T_{ex} is close to the temperature of the background radiation, which is the case for $T_{ex} \gtrsim 250$ K. The derived column densities can be a factor of up to $\sim$8 higher than derived from the pure absorption models for $b = 3$–10 km s^{-1}. This is still consistent with the non-detection of H^{13}CN which gives an upper limit of N(H^{13}CN) $< 6 \times 10^{15}$ cm^{-2}.

3.2. CO_2

As shown in Fig. 3, the gas-phase CO_2 $\nu_2 = 1$–0 band at 15.0 μm is clearly detected in absorption toward IRc2. The individual R- and P-branch lines are also detected in absorption. The CO_2 $\nu_2 = 2$–1 ro-vibrational band has not been detected, nor any lines of $^{13}CO_2$. In this case, both results with and without correction for the continuum of BN have been determined, since there are no prior data which indicate that the CO_2 absorption occurs only toward IRc2. Modeling of the CO_2 ν_2 band toward IRc2 without subtraction of the BN continuum results in $T_{ex} \sim 220$ K and $N \sim 5 \times 10^{16}$ cm^{-2}, assuming pure absorption, thermal excitation and a Doppler parameter of $b = 3$–10 km s^{-1}. Table 1 shows that these results are not sensitive to the adopted line width. When 62% of the BN continuum is subtracted, like in the case for HCN and C_2H_2, the ro-vibrational lines start to become optically thick for $b = 3$ km s^{-1}, resulting in a much larger column density at this line width. The excitation temperature in both cases lies in between those of HCN and C_2H_2, suggesting it might also originate in the plateau gas.

The effect of emission in the line has also been tested for CO_2, using an excitation model similar to that for HCN and C_2H_2, including levels up to $J = 40$ in both the $\nu_2 = 0$ and 1 vibrational state. For excitation temperatures equal to those in Table 1 emission in the line itself results in column densities that are $\lesssim$20% higher, which is within the error bars listed and therefore is not significant. This effect only becomes important for CO_2 for $T_{ex} \gtrsim 300$ K.

Table 2. IRc2 abundances compared with models and other massive YSOs.

	This work[a]	Carr et al. ('95)[a]	Submm obs[a,b]	IR obs.	Hot core models[c]	Envelope models[d]
	10^{-7}	10^{-7}	10^{-7}	10^{-7}	10^{-7}	10^{-7}
$N(HCN)/N(H_2)$	0.9–9.8	6.0–23	0.5–3.3	2[e]	~7–10	~0.1–0.9
$N(C_2H_2)/N(H_2)$	0.4–4.9	3.2–12	–	1[e]	~0.3–2	~0.02–0.2
$N(CO_2)/N(H_2)$	~3.3–125	–	–	2[f]	~10	~2–90
$N(CO_2)/N(H_2)$[g]	1.6–8.9	–	–	2[f]	~10	~2–90

[a] Using $N(H_2) = (0.8–3) \times 10^{23}$ cm^{-2}, corresponding to the line of sight column density (Evans et al. 1991).

[b] Average column density from Blake et al. (1987) and Schilke et al. (2001) for the plateau gas.

[c] HCN and C_2H_2 from Rodgers & Charnley (2001) for $t \sim 10^5$ yr at $T = 300$ K for HCN and $T = 100–300$ K for C_2H_2. CO_2 from Charnley (1997) at $T = 200$ K and $t \sim 10^5$ yr. It is assumed that HCN, C_2H_2, and CO_2 are not present originally in ices.

[d] After Doty et al. (2002) for $t \sim 10^5$ yr, and $T \sim 300$ K for HCN, $T \sim 200$ K for C_2H_2, and $T \sim 200–250$ K for CO_2. It is assumed that only CO_2 is present originally in ices and $\zeta = (1.3–5.6) \times 10^{-17}$ s^{-1} has been adopted.

[e] Average from Lahuis & van Dishoeck (2000).

[f] Average from Boonman et al. (2000).

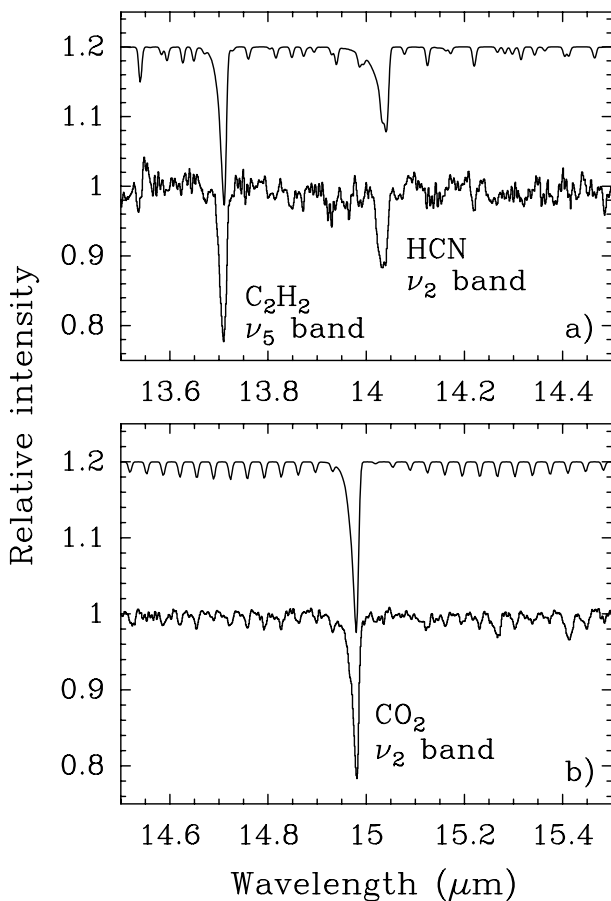[g] Without subtracting the BN continuum.

Fig. 3. a) Normalized spectrum of HCN and C_2H_2 toward IRc2 with 62% BN continuum subtracted (see text). The best fitting model for $b = 5$ km s^{-1} (see Table 1) shifted upward by 0.2, is shown for comparison. **b)** Normalized spectrum of CO_2 toward IRc2 with no continuum subtracted, together with the best fitting model spectrum for $b = 5$ km s^{-1} shifted upward by 0.2 (Table 1).

3.3. Abundances

Evans et al. (1991) and Wynn-Williams et al. (1984) argue from NH_3 maps that the line of sight toward IRc2 passes through the edge of the hot core, so that at most a small part of the hot core can be probed in absorption. In combination with the derived excitation temperatures, this suggests an origin in the plateau gas for all three molecules. Therefore the abundances are computed using $N(H_2) = (0.8–3) \times 10^{23}$ cm^{-2} corresponding to the line of sight column density found by Evans et al. (1991) from the depth of the silicate feature. Since the optical depth of the continuum between 13 and 15 μm rapidly becomes very high for larger H_2 column densities, these values are appropiate for (colder) gas probed in absorption in front of the $\tau_{cont} \sim 1$ location.

It should be noted that the HCN and C_2H_2 abundances are derived from pure absorption models, without including dust mixed with the gas. Given the complex nature of the IRc2/BN complex, determining a realistic physical structure to be used in radiative transfer models is not trivial. At present, the accuracy of the derived HCN and C_2H_2 abundances is best determined by comparison to observations at high spectral and spatial resolution, e.g. with TEXES (Lacy et al., in prep.).

The inferred HCN and C_2H_2 abundances are a few times 10^{-7} (Table 2). These are of the same order of magnitude as the values found for other massive protostars (Lahuis & van Dishoeck 2000). They also agree with those found by Blake et al. (1987) and Schilke et al. (2001) for HCN in the hot core and plateau gas. Stutzki et al. (1988) find similar abundances for HCN in the plateau gas from the $J = 9–8$ transition. The abundances are listed in Table 2.

Wright et al. (1996) mapped the HCN emission in the IRc2 region at ~6″ resolution using the BIMA interferometer. It shows no significant HCN emission at the position of BN, consistent with the absence of HCN absorption toward BN. They divide the plateau gas near IRc2 in three different chemical regions, an SiO-rich zone, an expanding shell rich in SO and SO_2

emission and a zone with high-velocity HCN emission extending over more than 50 km s^{-1}, which they attribute to evaporation of ices and ablation from pre-existing dense clumps. This could be a possible explanation for the high HCN abundance found from the absorption lines, which is an order of magnitude higher than found in the more extended Orion ridge (Bergin et al. 1997). The HCN and C_2H_2 abundances also agree well with predictions from hot core models by Rodgers & Charnley (2001). Abundances taken at a single temperature/density point from envelope models following Doty et al. (2002) are in agreement with the low end of the observed range (see Table 2 and Sect. 5.1 for details). Thus, the observed HCN and C_2H_2 probably originate in gas that has been blown away from the hot core clumps near IRc2 and now resides in the plateau gas in the swept-out cavities between the hot core clumps (see Fig. 1). This is in agreement with Carr et al. (1995), who ascribe their observed ro-vibrational HCN and C_2H_2 absorption lines to the plateau gas.

Based on the fact that CO_2 absorbs in the same wavelength region as HCN and C_2H_2 and has the same excitation temperature, it is likely that the observed CO_2 does not originate in the hot core itself, although it still can contain large amounts of hidden CO_2. Since no previous CO_2 observations with smaller beam sizes exist, it is difficult to determine whether the CO_2 is confined to a region close to the hot core like HCN and C_2H_2 or whether it is more widespread. The gas-phase CO_2 abundance, assuming it is seen both in the direction of IRc2 and BN, is of the same order as those of HCN and C_2H_2 (Table 2). It is somewhat higher than the values found for some other massive YSOs (van Dishoeck et al. 1996; van Dishoeck 1998; Boonman et al. 2000). Assuming CO_2 is observed only in the direction of IRc2, like HCN and C_2H_2, the derived abundances are ~(0.3–3) × 10^{-6} for b = 10 km s^{-1} and ~10^{-5} for b = 3 km s^{-1}. This is of the same order of magnitude as the CO_2 ice abundance of $N(CO_2)/N(H_2)$ ~ (0.4–3) × 10^{-6} toward IRc2 and agrees also with the CO_2 ice abundances found toward other massive protostars (Gerakines et al. 1999). The same is true if CO_2 is seen both in the direction of IRc2 and BN. This suggests that most of the CO_2 ice in the neighborhood of IRc2/BN must have evaporated off the grains. In both cases the CO_2 abundances also show reasonable agreement with both the models from Charnley (1997) and Doty et al. (2002) listed in Table 2. This indicates that the observed gas-phase CO_2 abundances are explained best by a combination of pure gas-phase chemistry and grain-mantle evaporation.

4. Molecular emission toward Peak 1 and Peak 2

Contrary to what is observed for IRc2, the CO_2 ν_2 = 1–0 band is seen in emission toward both Peak 1 and 2 (Fig. 4). HCN and C_2H_2 are also seen in emission but only toward Peak 2, although the non-detection toward Peak 1 could be due to the higher noise level there. The shape of the CO_2 Q-branch toward Peak 1 and Peak 2 is very similar to that seen in absorption toward IRc2 (Fig. 5). In order to investigate whether the similarities and differences between both positions and IRc2 are true physical and/or chemical differences or whether they are due to geometrical and radiative transfer effects, we follow the same
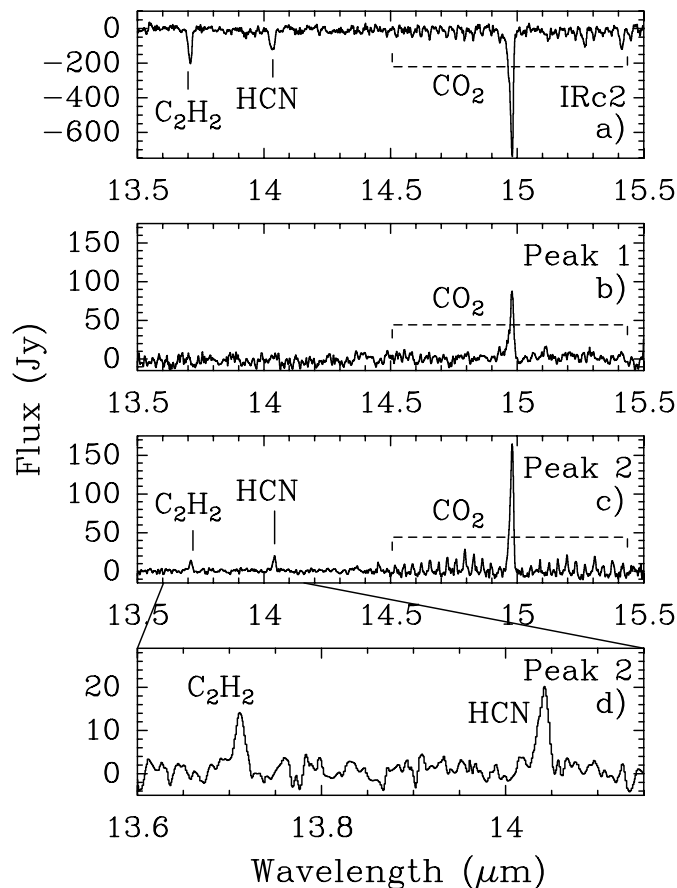

Fig. 4. Continuum subtracted spectra of CO_2, C_2H_2 and HCN toward **a)** Orion-IRc2, **b)** Peak 1, and **c)** Peak 2. **d)** Blow-up of the 13.6–14.15 μm region toward Peak 2.

analysis as in González-Alfonso et al. (2002; hereafter GA02). They discuss the CO and H_2O ro-vibrational bands toward the same three positions and find the same striking similarities between the Peak 1 and Peak 2 spectra as is found here for CO_2. GA02 also investigate in detail the excitation mechanisms and show that radiative pumping, rather than collisional excitation, likely dominates. The comparison with CO may allow accurate relative abundances in the shocked gas to be determined. The resulting CO_2/CO ratio can then be compared with predictions from chemical models.

4.1. Radiative transfer model

A radiative transfer model has been constructed to investigate optical depth effects of the emission toward Peak 1 and Peak 2. In this model the source is represented as a slab of thickness d, divided in a number of smaller sheets, each with the same constant H_2 density and gas temperature. For CO_2, levels up to J = 40 in the ground and ν_2 = 1 vibrational states have been included. For HCN and C_2H_2, levels up to J = 21 and J = 24 respectively, are included in both vibrational states. Once the level populations are known, the radiative transfer can be calculated, including emission and absorption by both lines and continuum. In the next paragraphs, three different scenarios will be discussed. Scenario 1 considers radiative
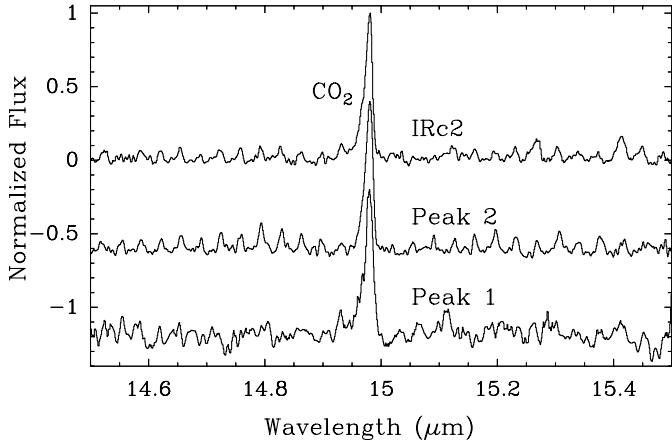
Fig. 5. Comparison of the CO_2 ν_2 band shape toward IRc2, Peak 1 and Peak 2. The CO_2 absorption toward IRc2 has been inverted to an emission spectrum. All continuum subtracted spectra have been normalized with respect to their own peak flux. The Peak 2 spectrum is shifted by -0.6 and the Peak 1 spectrum by -1.2.
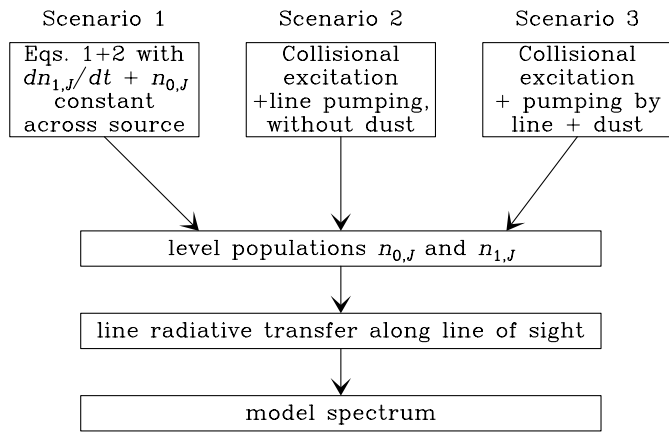

Fig. 6. Schematic representation of the scenarios discussed in Sect. 4.

pumping of the molecules by the IRc2/BN complex. Scenario 2 assumes that the molecules are excited by collisions only, which would be the case if the shock itself is the dominant excitation mechanism. Finally, scenario 3 discusses the possibility of excitation by infrared radiation from dust mixed with warm gas. Following the discussion in GA02, first the excitation rates in the case of scenario 1 and 2 are compared, in order to determine the relative importance of radiative versus collisional excitation.

4.2. Radiative versus collisional excitation rates

If it is assumed that the CO_2 gas toward Peak 1 and Peak 2 is excited predominantly by radiation from a source of temperature T_s and effective radius r_s located in the IRc2/BN complex and subsequently emits toward the observer, the radiative excitation rate from the $\nu_2 = 0$ state to the ($\nu_2 = 1, J_1$) level (in cm^{-3} s^{-1}) is given by (cf. Eq. (6) in GA02)

$$\frac{dn_{1,J_1}}{dt} = \frac{r_s^2}{4r^2} g_{1,J_1} 10^{-0.4\mathcal{A}_{15.0}} \left[\frac{A_{J_1}^R}{\exp\{h\nu_{J_1}^R/(kT_s)\} - 1} \frac{n_{0,J_1-1}}{g_{0,J_1-1}} \right.$$
$$\left. + \frac{A_{J_1}^Q}{\exp\{h\nu_{J_1}^Q/(kT_s)\} - 1} \frac{n_{0,J_1}}{g_{0,J_1}} + \frac{A_{J_1}^P}{\exp\{h\nu_{J_1}^P/(kT_s)\} - 1} \frac{n_{0,J_1+1}}{g_{0,J_1+1}} \right], \quad (1)$$

where r is the distance between the exciting source and the emitting CO_2 molecules, $g_{0,J}$ is the total statistical weight of the $(v = 0, J)$ level, $\mathcal{A}_{15.0}$ is the extinction at 15.0 μm along that path, A_J^R, A_J^Q, A_J^P are the Einstein-A coefficients for the $R(J-1)$, $Q(J)$, $P(J+1)$ ro-vibrational lines, respectively, ν_J^R, ν_J^Q, ν_J^P the corresponding line frequencies and $n_{0,J}$ the density in the $(v = 0, J)$ level. The total statistical weight in the $(v = 0, J)$ level is $2J+1$, whereas that of the $(v = 1, J)$ level is $2(2J+1)$. The same formulae also apply to C_2H_2 and HCN.

For the populations of the levels in the $v = 0$ state, a Boltzmann distribution has been adopted at $T = 300$ K, the best-fit temperature for the warm component toward Peak 1 and Peak 2 as determined from the CO ro-vibrational band at 4.7 μm by GA02. Using the CO_2 excitation temperature found for IRc2 (Table 1) does not change the results significantly.

For Peak 1 it is assumed that BN is the dominant excitation source and that the extinction along the line of sight from BN to Peak 1 at 15.0 μm is zero. For T_s, a value of 500 K is adopted consistent with the derived color temperature for BN from Gezari et al. (1992). The radius of the stellar source r_s has been adjusted so that the flux at 15 μm at a distance of 450 pc is $\sim$1300 Jy, corresponding to the interpolation of the dereddened 12 μm and 20 μm fluxes listed by Gezari et al. (1992). The exact choice of T_s and r_s is not important as long as the emerging flux at 450 pc is fixed to $\sim$1300 Jy. A distance between the CO_2 molecules and BN of $r \sim 10^{17}$ cm is adopted, corresponding to the angular distance of 15″ between Peak 1 and BN. Other infrared sources in the Orion BN/KL region might also contribute to the radiative pumping of Peak 1. Since these sources are less luminous than BN at this wavelength and located farther from Peak 1 their contribution will change the total radiative pumping rate from the $\nu_2 = 0$ to the $\nu_2 = 1$ state by at most a factor of $\sim$2.

Although BN is the dominant infrared source in the 13.5–15.5 μm range (Gezari et al. 1992), for Peak 2 IRc2 is much closer. Therefore it is assumed that the exciting source for Peak 2 is located at the position of IRc2 at $r \sim 1.6 \times 10^{17}$ cm. The dereddened flux of IRc2 at $\sim$15 μm is $\sim$650 Jy, but in order to account for a possible contribution of other sources close to IRc2 with comparable infrared fluxes, a flux of twice this value is used, corresponding to a BN type source at the position of IRc2 (Gezari et al. 1992). Therefore the same values for T_s and r_s used for Peak 1 are used for Peak 2. Assuming instead a flux of $\sim$3400 Jy, equal to the observed ISO-SWS flux toward IRc2/BN at a distance in between BN and IRc2, does not change the total pumping rate by more than a factor of $\sim$2.

Alternatively, if collisions excite the $\nu_2 = 1$ state of CO_2 the excitation rate (in s^{-1}) is given by the product $n(X) k_{0-1}^{CO_2-X}$, where $n(X)$ is the density of the collision partner X and k_{0-1}

the collisional excitation rate coefficient from the $\nu_2 = 0$ to the $\nu_2 = 1$ state. A discussion on the collisional rate coefficients for CO_2 is given in Appendix A. Based on that discussion only H_2 will be considered as a collision partner.

Using fractional populations in Eq. (1) and adopting a hydrogen density of $n(H_2) = 2 \times 10^7$ cm^{-3}, corresponding to the density in the warm component of the shock (GA02), the radiative and collisonal pumping rates (in s^{-1}) can be compared directly. Figure 7 shows the ratio of these rates for CO_2 in Peak 1 and Peak 2, but the curves can easily be scaled to other densities. It can be seen that for kinetic temperatures $T \sim 150$–300 K radiative pumping is comparable to collisional excitation, for both Peak 1 and Peak 2. However, the line of sight between the exciting source and Peak 1/2 may not be in the plane of the sky, thus underestimating the actual distance. In that case the radiative pumping rate used is too high. Also, the extinction along the line connecting the exciting source and Peak 1/2 is probably small, but not zero, again indicating that the radiative pumping rates used are too high. Together this suggests that, for $T \gtrsim 200$ K radiative excitation by infrared sources in the IRc2/BN complex is not the dominant excitation mechanism for CO_2, contrary to what is the case for CO (GA02). As will be shown below, radiative pumping by warm dust mixed with the warm gas at the Peak 1 and 2 positions may be still significant. If the CO_2 is located in the hot component at $T \sim 3000$ K, collisions become more important, because of the higher kinetic temperature of the gas.

The HCN–H_2 and C_2H_2–H_2 collisional rates are not known. Because the vibrational energy and reduced mass of HCN and C_2H_2 are close to those of CO_2, their collisional rates will be approximately the same as those for CO_2. Adopting the same collisional de-excitation rates as for CO_2 the ratio of the radiative and collisional rates are calculated for HCN and C_2H_2 in the same way as for CO_2. Figure 7 shows that also for HCN and C_2H_2 the radiative and collisional excitation rates are comparable for $T = 150$–300 K, although for C_2H_2 the ratio is higher than for CO_2 and HCN, due to its larger Einstein-A coefficient.

4.3. CO_2

4.3.1. Scenario 1: Radiative excitation by IRc2/BN

Using Eq. (1) and adopting the same rotational excitation temperature for the $\nu_2 = 0$ state as in Sect. 4.1, the density of the $(\nu_2 = 1, J_1)$ level n_{1,J_1} can be calculated from

$$n_{1,J_1} = \left[A_{J_1}^P + A_{J_1}^Q + A_{J_1}^R\right]^{-1} \frac{dn_{1,J_1}}{dt}. \tag{2}$$

The density of $n(H_2) = 2 \times 10^7$ cm^{-3} in the warm component of the shock (GA02) is lower than the critical density for collisional de-excitation, so that the de-excitation of the levels will be dominated by radiation. The ratio of the densities for the $\nu_2 = 1$ state with those of the $\nu_2 = 0$ state gives the vibrational excitation temperature. In the case of radiative excitation this vibrational excitation temperature varies with the distance r from the exciting source, described in Sect. 4.2.

Using Eqs. (1) and (2), the CO_2 vibrational excitation temperature T_{vib} for Peak 1 varies from ~65–110 K within the
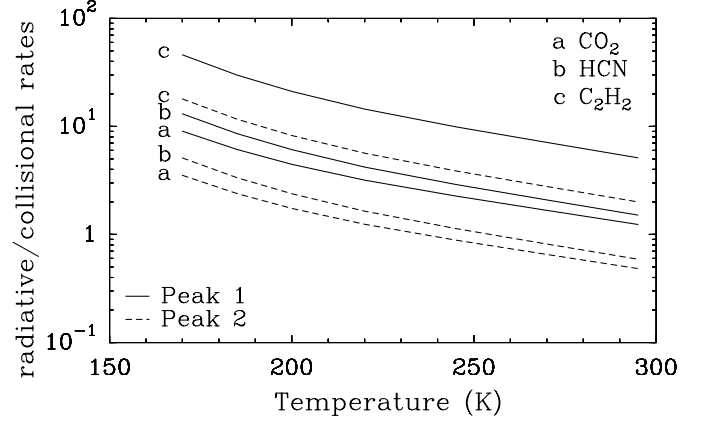

Fig. 7. Estimated ratio of the radiative to collisional excitation rates for CO_2, HCN and C_2H_2 in Peak 1 and Peak 2 as functions of the kinetic temperature T. The radiative excitation rates per molecule are computed from Eq. (1), assuming zero extinction and summing over all $\nu_2 = 1$ rotational levels. Only H_2 is considered as collision partner with an adopted density of 2×10^7 cm^{-3}, corresponding to the density of the warm component of the shock (GA02).

ISO-SWS beam and for Peak 2 from ~63–80 K (Figs. 8 and 9). Assuming a constant vibrational temperature, corresponding to a constant radiative pumping rate within the ISO-SWS beam, together with a constant CO_2 abundance and H_2 density and a constant rotational excitation temperature in the $\nu_2 = 0$ state, the level populations are known and thus a synthetic spectrum can be calculated. It should be noted that in this case the level populations are not calculated self-consistently with the radiative transfer. An H_2 density of 2×10^7 cm^{-3} has been adopted, whereas the thickness of the slab has been chosen such that the integrated column density across the slab is $N(H_2) = 1 \times 10^{22}$ cm^{-2} for Peak 1 and $N(H_2) = 7 \times 10^{22}$ cm^{-2} for Peak 2, corresponding to the values for the warm component of the shock listed by Rosenthal et al. (2000) and Wright (2000), respectively.

The CO_2 abundance and the rotational excitation temperature in the $\nu_2 = 0$ state have then been varied to find a good match to the observed CO_2 emission. These calculations have been done for different values of T_{vib} within the SWS beam. The results are shown in Figs. 8 and 9.

For Peak 1 it is found that the Q-branch is well fit with a rotational temperature of ~150–225 K, as long as the lines are not too optically thick (i.e. $\tau \lesssim 5$). For line widths in the range of $b = 3$–10 km s^{-1} this is the case for $T_{vib} \gtrsim 75$ K, corresponding to $r \lesssim 1 \times 10^{17}$ cm. Lower vibrational temperatures require lower rotational temperatures to fit the CO_2 Q-branch, but then huge CO_2 column densities $\int n(CO_2)dr > 10^{19}$ cm^{-2} are needed to match the observed flux and the P- and R-branches then exceed the 3σ upper limit derived from the SWS spectra.

Since Peak 2 is located further from the IRc2/BN complex the vibrational temperatures within the ISO-SWS beam due to radiative excitation are somewhat lower. Following the same approach as for Peak 1, the CO_2 Q-branch toward Peak 2 is fit best with a rotational temperature of $T_{rot} \sim 150$ K for $\tau \lesssim 5$, which is the case for $T_{vib} \gtrsim 80$ K and $b = 3$–10 km s^{-1}. This is outside the observed range of T_{vib} within the ISO-SWS

beam (Fig. 9). This figure also shows that the CO_2 emission toward Peak 2 cannot be explained by radiative excitation by the IRc2/BN complex, unless very large column densities are involved. The rotational temperature of $T_{rot} \sim 150$ K is in excellent agreement with the temperature derived by Wright (2000) for the H_2 lines in the warm component of the shock. This suggests that CO_2 and H_2 are co-located.

The same analysis has been performed for CO in the warm component of the shock allowing the determination of the CO_2/CO ratio for comparison with chemical models. Here, the CO vibrational excitation temperatures from GA02 are used, as a function of the distance from the exciting source. The CO column density found from these models at the position of Peak 1 ($r = 1 \times 10^{17}$ cm) is consistent with that found by GA02. Comparison of the CO_2 column densities for Peak 1 with those of CO gives a CO_2/CO ratio of ~ 0.3 as long as the optical depth of the CO_2 lines is comparable to that of the CO lines (i.e. for $\tau \lesssim 5$). These conditions are met for $r \lesssim 1 \times 10^{17}$ cm, i.e. between BN and Peak 1. Since for Peak 2 the CO_2 emission cannot be fit well for $T_{vib} < 80$ K due to high optical depths, no CO_2/CO can be derived within the SWS beam in the case of radiative excitation by the IRc2/BN complex. For $T_{vib} \geq 80$ K, which is outside the SWS beam, a ratio of CO_2/CO ~ 0.6 is found (Table 3).

Fig. 8. Peak 1 vibrational excitation temperature (left axis) versus distance from BN for the physical model described in Sect. 4.2. The column densities of the best fitting models for CO_2 (right axis) are shown by the dots, assuming no background radiation, $b = 10$ km s^{-1} and a constant vibrational excitation temperature in the SWS beam as a function of radius. The x-coordinates of the dots refer to the radii at which the value of T_{vib} listed between parentheses occur. The optical depth of the most optically thick CO_2 ro-vibrational transition of the ν_2 band is also listed. The position of the SWS beam w.r.t. BN is indicated.

4.3.2. Scenario 2: Collisional excitation

In order to investigate optical depth effects in the case of collisional excitation of CO_2, the same radiative transfer model has been used, but the level populations in both vibrational states are calculated with the Accelerated Monte Carlo method by Hogerheijde & van der Tak (2000), using the collisional excitation rates from Fig. A.1 for the same slab model as described before and including no infrared pumping. Kinetic temperatures of $T = 150$–200 K for Peak 1 and $T = 150$ K for Peak 2 have been used, corresponding both to the rotational temperatures derived from the CO_2 emission and the temperature of warm H_2 gas as derived by Wright (2000) for Peak 2, and estimated for Peak 1 by Rosenthal et al. (2000). The resulting level populations indicate a vibrational excitation temperature of ~ 78 K at $T = 150$ K and ~ 87 K at $T = 200$ K. The CO_2 abundances with respect to H_2, $n(CO_2)/n(H_2)$, found for collisional excitation are shown in Table 3. The optical depth in this case is ~ 1. These abundances are lower than in the case of radiative excitation by the IRc2/BN complex at the same vibrational temperature.

4.3.3. Scenario 3: Excitation by warm dust

A third, preferred possibility is that infrared radiation from warm dust mixed with the shocked gas can excite the molecules. In order to investigate this effect, the level populations are calculated using the same method as in the case of collisional excitation, but now including infrared pumping by dust, using grain opacities from Ossenkopf & Henning (1994) and assuming the dust temperature is close to the kinetic temperature. For Peak 2 also models with a dust temperature of
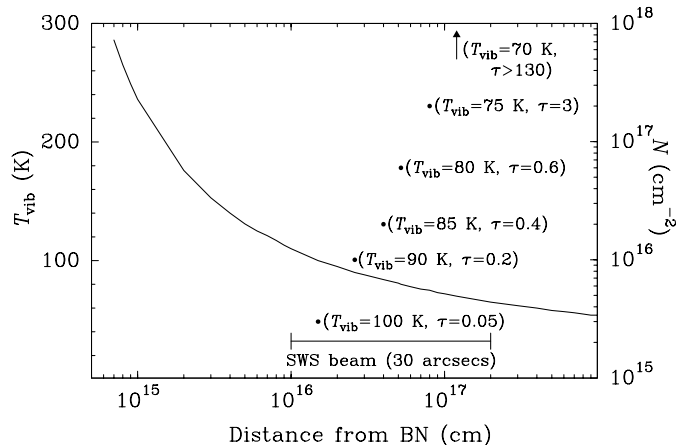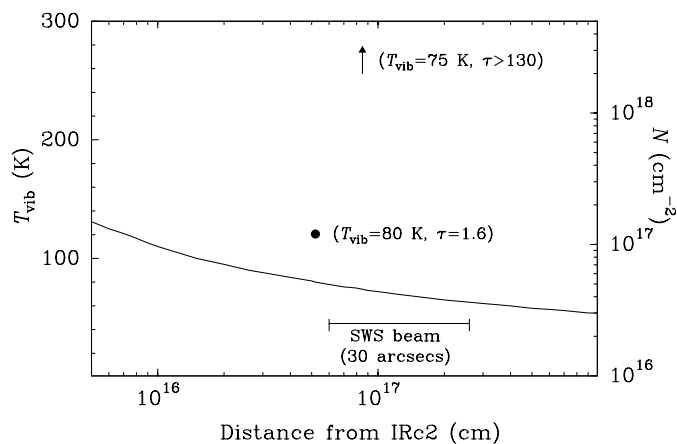
Fig. 9. Same as Fig. 8 but now for Peak 2. The source that is radiatively exciting the CO_2 molecules is the same as described in Sect. 4.2.

100 K have been investigated, corresponding to the color temperature around 15 μm toward Peak 2. For Peak 1 the color temperature is ~ 150 K. The resulting abundances with respect to H_2 are shown in Table 3. These abundances are significantly lower than those for collisional excitation only, indicating that if dust is mixed with the gas, the CO_2 will be radiatively excited. Since the color temperatures of the dust around 15 μm towards both Peak 1 and 2 are comparable to the kinetic temperature of the warm H_2 gas and the rotational temperature of the CO_2 emission, it is likely that dust is mixed with the gas in the warm component of the shock. The pumping rates by this warm dust are much higher than those by the IRc2/BN complex resulting in much lower abundances.

4.4. HCN and C_2H_2

The same three scenarios discussed for CO_2 have been investigated for the HCN and C_2H_2 emission detected toward Peak 2. In the case of radiative excitation by the IRc2/BN complex (scenario 1), it is found that the vibrational excitation temperature within the SWS beam ranges from ~67 K to ~83 K for HCN. For $\tau \lesssim 5$ the width of the HCN Q-branch is well-fit with a rotational temperature of ~50–125 K for b = 3–10 km s^{-1}. This is the case for $T_{vib} > 70$ K. For lower T_{vib} the rotational temperature decreases to ~20 K and large column densities ($\geq 3 \times 10^{17}$ cm^{-2}) are required to match the Q-branch, since the optical depth increases rapidly. Such high column densities are not observed in the extended ridge or plateau gas, which match the derived rotational temperature. Therefore it is likely that the HCN emission is not very optically thick. Since no HCN has been detected toward Peak 1, only upper limits have been determined. Comparison of the HCN column densities with those of CO in the case of scenario 1 results in an HCN/CO ratio of ~0.01–0.1 for Peak 2 and $\lesssim 0.1$ for Peak 1 (Table 3). For C_2H_2 the vibrational temperature within the SWS beam ranges from ~73 K to ~90 K. The Q-branch is matched best with a rotational temperature of ~50–175 K for b = 3–10 km s^{-1}. As for HCN, this is the case for $T_{vib} > 70$ K and the same conclusions are found. The results are listed in Table 3.

Scenarios 2 and 3, considering collisional excitation in the warm component of the shock and excitation by dust mixed with the warm gas respectively, have also been investigated. The results are included in Table 3.

Since both the HCN and C_2H_2 Q-branches toward Peak 2 are much weaker than that of CO_2, their rotational temperature is less well-constrained. The derived temperature range of ~50–175 K indicates that an origin in the colder extended ridge is also possible. Assuming collisional excitation at $T_{kin} = 50$ K, corresponding to the temperature of the extended ridge, the observed emission for both HCN and C_2H_2 could not be reproduced. Similarly, including dust at 50 K could also not reproduce the observed emission for both molecules.

As a final possibility, the slab model for the warm component of the shock has been used, with the assumption that no HCN and C_2H_2 is present. Then, a slab of cold gas at $T = 50$ K has been placed in front of it, such that the total column density across the whole slab is $N(H_2) \sim 3 \times 10^{23}$ cm^{-2} corresponding to the value derived by Sutton et al. (1995) for the extended ridge. In this case the warm dust pumps the cold HCN and C_2H_2, resulting in abundances of a few times 10^{-7} for both HCN and C_2H_2. These are similar to those derived in the case of collisional excitation in the warm component of the shock. They are also similar to those in the case of radiative excitation by the IRc2/BN complex, using the same H_2 column density. But they are much higher than in the case of radiative excitation by dust mixed with gas in the warm component of the shock (Table 3).

Thus, if HCN and C_2H_2 originate in the warm component of the shock, the most likely excitation mechanism is by infrared radiation from dust mixed with the warm gas (scenario 3), since the pumping rates in this case are much higher than in the other cases. If they originate in the extended ridge

they are probably excited by radiation from the IRc2/BN complex and/or dust of the warm component of the shock lying behind the extended ridge.

4.5. Comparison with chemical models

The previous sections show that the CO_2 emission toward Peak 1 and Peak 2 does not arise in the hot component of the shock at $T \sim 3 \times 10^3$ K, but probably arises in gas of $T \sim 150$–200 K, consistent with conditions in the warm component of the shock. Three different scenarios have been calculated, with the inferred CO_2 abundances differing by more than four orders of magnitude (Table 3).

Comparing the derived CO_2/CO ratios for Peak 1 and Peak 2 of $\gtrsim 0.3$ in the case of radiative excitation by the IRc2/BN complex (scenario 1) with the shock models by Charnley & Kaufman (2000) shows that this ratio is much higher than their post-shock value of CO_2/CO $\sim 5 \times 10^{-5}$ for a shock that destroys the CO_2 without reformation in the gas-phase (i.e. $v_{shock} \gtrsim 30$ km s^{-1}, $n_H > 10^5$ cm^{-3}). These results are listed in Table 3. If the CO_2 is totally destroyed in either a shock or a flaring event then the CO_2 will be reformed through gas-phase reactions increasing to abundances CO_2/CO of $\lesssim 10^{-2}$ at $t \sim 10^5$ yr for $T = 200$ K. (Charnley & Kaufman 2000; Doty et al. 2002). This is still at least one order of magnitude lower than the CO_2/CO ratio found above. Additionally, the time since the passage of the shock is estimated to be much shorter than 10^5 yr, about ~10^3–10^4 yr (Genzel & Stutzki 1989; Wilson et al. 1986). This shows that the abundances found in the case of radiative excitation by the IRc2/BN complex cannot be explained by reformation in the gas-phase after destruction of the CO_2 in the shock. In fact, such high CO_2 abundances have not been reported in any other star-forming regions, making it unlikely that the IRc2/BN complex is the exciting source.

In the preferred case of scenario 3 where the CO_2 is radiatively excited by warm dust mixed with the gas, the derived abundances are in agreement with predictions for quiescent warm gas at $t \lesssim 10^4$ yr (Doty et al. 2002). Here the Doty et al. (2002) models are used as generic high-temperature models. They are also in good agreement with predictions from Charnley & Kaufman (2000) for a shock that destroys the CO_2, with little or no reformation through gas-phase reactions on time scales of $t \lesssim 10^4$ yr. In the case of collisional excitation of CO_2 in the warm component of the shock (scenario 2), the abundances with respect to H_2 are in agreement with the predictions from the chemical models by Doty et al. (2002) at $t \sim 10^4$ yr. But, as argued in Sect. 4.3.3, it is likely that dust is present in the warm component of the shock, making scenario 3 the most likely excitation mechanism for CO_2.

Contrary to CO_2, the origin of the HCN and C_2H_2 gas is more difficult to establish. In the case of radiative excitation by the IRc2/BN complex (scenario 1) the HCN/CO and C_2H_2/CO ratios are very high compared to predictions from chemical models of HCN/CO $\lesssim 3 \times 10^{-5}$ and C_2H_2/CO $\lesssim 3 \times 10^{-5}$ for $T < 200$ K (Doty et al. 2002). On the other hand, comparison with H_2, using $N(H_2) \sim 3 \times 10^{23}$ cm^{-2} from Sutton et al. (1995) for the extended ridge, abundances of ~10^{-7} for HCN

Table 3. Peak 1 and Peak 2 abundances including optical depth effects and stimulated emission compared with predictions from chemical models.

	Peak 1	Peak 2	CK 2000[b]	Doty02[c]
	Scenario 1: Excitation by IRc2/BN			
	$T = 200-400$ K[a]			
CO_2/CO	~0.3	~0.6	~5(−5)	~2(−4) − 8(−3)
HCN/CO	≲0.1	~0.01−0.1	−	≲3(−5)
C_2H_2/CO	≲0.01	~0.01	−	≲3(−5)
CO_2/H_2	~2(−4)	>1(−4)	~1(−8)	~6(−8) − 3(−6)
HCN/H_2	<2(−7)	~7(−7)	−	≲1(−8)
C_2H_2/H_2	<1(−8)	~1(−7)	−	≲1(−8)

	Peak 1		Peak 2	Doty02[c]
	Scenario 2: Collisional excitation, no dust included			
	$T_{kin} = 150$ K	$T_{kin} = 200$ K	$T_{kin} = 150$ K	
CO_2/H_2	4(−6)	1(−6)	1(−6)	~6(−8) − 3(−6)
HCN/H_2	<3(−6)	<6(−7)	3(−7)	≲1(−8)
C_2H_2/H_2	<3(−6)	<7(−7)	3(−7)	≲1(−8)

	Peak 1		Peak 2		Doty02[c]
	Scenario 3: Excitation by warm dust mixed with gas				
	$T_{kin} = 150$ K	$T_{kin} = 200$ K	$T_{kin} = 150$ K	$T_{kin} = 150$ K	
	$T_{dust} = 150$ K	$T_{dust} = 200$ K	$T_{dust} = 150$ K	$T_{dust} = 100$ K	
CO_2/H_2	3(−8)	6(−9)	3(−9)	6(−8)	~6(−8) − 3(−6)
HCN/H_2	<6(−9)	<2(−9)	4(−10)	1(−8)	≲1(−8)
C_2H_2/H_2	<4(−9)	<9(−10)	2(−10)	7(−9)	≲1(−8)

$a(b)$ denotes $a \times 10^b$.

[a] Temperature of the warm component of the shock and assuming radiative excitation.

[b] Charnley & Kaufman (2000) for a shock that destroys the CO_2, without reformation through gas-phase reactions.

[c] Doty et al. (2002) at $T \sim 150$–200 K and $t \sim 10^4$ yr for CO_2 and at $T < 200$ K, $t \lesssim 10^5$ yr for HCN and C_2H_2. It is assumed that these molecules are originally not present in ices.

and C_2H_2 are found. Similar abundances are obtained when it is assumed that dust in the warm component of the shock excites the molecules in the much cooler extended ridge. These are higher than predicted by gas-phase models at $T \lesssim 200$ K, which predict abundances of $\lesssim 5 \times 10^{-8}$ at late times. For $T \gtrsim 200$ K HCN and C_2H_2 abundances of ~10^{-7} are easily produced by gas-phase models (Rodgers & Charnley 2001; Doty et al. 2002). The HCN abundance is also higher than the values of ~10^{-8} derived from submillimeter observations by Blake et al. (1987) and Schilke et al. (1992) for the extended ridge. Together this makes both scenarios less likely excitation mechanisms. Moreover, as noted in Sect. 4.3.3 and above, warm dust is likely mixed with the gas.

The HCN and C_2H_2 abundances found in the case of the preferred scenario 3 are in agreement with predictions from gas-phase models for $T < 200$ K and $t \lesssim 10^5$ yr (Doty et al. 2002) (Table 3). The HCN abundance is also in good agreement with the predicted abundances from chemical models for the Orion shock of a few times 10^{-9} by Schilke et al. (1992) which also explains their value derived from HCN $J = 1$–0 observations in the direction of Peak 1. This may indicate that HCN and C_2H_2 are destroyed by the shock. On the other hand, Blake et al. (1987) find HCN abundances of ~5×10^{-9} for the

extended ridge, similar to what is found when HCN and C_2H_2 originate in the warm component of the shock. Therefore, it is also possible that HCN and C_2H_2 have been heated to temperatures $T \gtrsim 50$ K only recently ($t \lesssim 10^4$ yr), so that enhanced gas-phase formation has not yet taken place.

In summary, scenario 3 seems to be the preferred scenario for all three molecules, but in the case of HCN and C_2H_2 an origin in the extended ridge, based on the derived excitation temperatures, cannot be completely excluded. Mapping of the 13–15 μm continuum at high angular resolution could provide further evidence for the presence of warm dust toward Peak 1 and 2, and thus strengthen the case for scenario 3. In addition, infrared observations of HCN and C_2H_2 toward Peak 1 and 2 at high spectral resolution, e.g. with TEXES (see Sect. 3.1), will be useful to discriminate between an origin in the extended ridge or the warm component of the shock.

5. IRc2 versus Peak 1/2

5.1. HCN and C_2H_2

HCN abundances as high as 10^{-6} as found toward IRc2 (Table 2) cannot be explained adequately by steady-state

Table 4. IRc2 versus Peak 1/2 abundances compared with chemical models.

	IRc2/BN complex	Peak 1[a]	Peak 2[a]	CK2000[b]	Doty02[c]	Hot core models[d]
	10^{-7}	10^{-7}	10^{-7}	10^{-7}	10^{-7}	10^{-7}
CO_2/H_2	1.6–8.9[e]	0.06–0.3	0.03–0.6	~1–7	~0.6–30	~10
HCN/H_2	0.9–9.8	<0.06	0.004–0.1	–	$\lesssim 0.1$	~7–10
C_2H_2/H_2	0.4–4.9	<0.04	0.002–0.07	–	$\lesssim 0.1$	~0.3–2

[a] Using our preferred scenario 3 for excitation by warm dust mixed with the gas in the warm component of the shock (see Table 3 and Sect. 5).

[b] Charnley & Kaufman (2000) for reformation through gas-phase reactions at $T \sim 200$ K and $t \sim 10^4$ yr after destruction by a shock.

[c] Doty et al. (2002) at $T \sim 150$–200 K and $t \sim 10^4$ yr for CO_2 and at $T < 200$ K, $t \lesssim 10^5$ yr for HCN and C_2H_2. It is assumed that these molecules are originally not present in ices.

[d] HCN and C_2H_2 from Rodgers & Charnley (2001) for $t \sim 10^5$ yr at $T = 300$ K for HCN and $T = 100$–300 K for C_2H_2. CO_2 from Charnley (1997) at $T = 200$ K and $t \sim 10^5$ yr. It is assumed that HCN, C_2H_2, and CO_2 are not present originally in ices.

[e] Without subtracting the BN continuum (Table 2).

low-temperature gas-phase chemical models (Evans et al. 1991). As argued by van der Tak et al. (1999), not only grain-mantle evaporation but also high-temperature gas-phase chemistry plays a role in producing high HCN abundances in hot cores. The observed abundances toward IRc2 are consistent with predicted HCN abundances of up to $\sim 10^{-6}$ from pure gas-phase chemistry at $T > 200$ K (Doty et al. 2002; Rodgers & Charnley 2001).

The observed C_2H_2 abundance of $\sim 10^{-7}$ toward IRc2 is higher than the predicted abundances of $\sim 10^{-8}$ for pure gas-phase chemistry at $T \sim 200$ K by Doty et al. (2002), but their formation route for C_2H_2 is through reactions of water with $C_2H_3^+$ instead of dissociative recombination. Pure gas-phase models by Rodgers & Charnley (2001) do predict C_2H_2 abundances up to 10^{-7} for $T = 100$–300 K. The observed C_2H_2 abundance is also consistent with the upper limits found in interstellar ices of $<10^{-5}$ (Boudin et al. 1998) and its detection in cometary ices at an abundance of 0.1–0.9% with respect to H_2O (Brooke et al. 1996; Bockelée-Morvan et al. 2000), corresponding to abundances with respect to H_2 of $\sim 10^{-7}$. Therefore evaporation from grain mantles could also explain the observed C_2H_2 abundance toward IRc2.

The widths of the HCN and C_2H_2 ro-vibrational bands toward Peak 2 are somewhat smaller than those toward IRc2, suggesting a different origin. Also, much lower abundances are found in the preferred scenario 3, consistent with destruction of these molecules in the shock or heating on short time scales (see Sect. 4.5). Therefore, the HCN and C_2H_2 toward IRc2 probably originate in gas that has been blown away from the hot core clumps and now resides in the plateau gas in the swept-out cavities between these clumps, probing hot-core chemistry (see Sect. 3.3), whereas the HCN and C_2H_2 toward Peak 2 probably probe either shock chemistry or quiescent gas-phase chemistry at $T \lesssim 200$ K.

5.2. CO_2

The excitation temperature estimated from the CO_2 emission indicates that the CO_2 toward Peak 1 and Peak 2 does not originate in the hot component of the shock at $T \sim 3000$ K.

The results of Sect. 4.3 suggest an origin in the warm component of the shock. If the CO_2 toward Peak 1 and Peak 2 originates in this so-called plateau gas, then it is likely that the CO_2 absorption toward IRc2 also arises in this plateau gas, given the similar excitation temperatures and line widths. In that case the CO_2 absorption will be seen toward both IRc2 and BN contrary to what is observed for HCN and C_2H_2. Therefore the CO_2 ro-vibrational absorption band probably probes different gas and thus a different chemistry than the HCN and C_2H_2 ro-vibrational absorption bands toward IRc2.

Charnley & Kaufman (2000) show that C-shocks with speeds above ~ 30 km s^{-1} in regions with $n_H > 10^5$ cm^{-3} can efficiently destroy CO_2 after it is sputtered off the grains by the shock, converting it into CO. These physical conditions are approximately met in the Orion outflow (Chernoff et al. 1982; Schilke et al. 1992). The CO_2 emission toward Peak 2 is stronger than toward Peak 1, whereas the opposite is the case for CO in the hot component of the shock (GA02). This could suggest that the CO_2 gas has been destroyed more efficiently toward Peak 1 than toward Peak 2.

If the CO_2 is destroyed completely in the shock, the predicted abundances are lower than the observed gas-phase CO_2 abundances toward the IRc2/BN complex and Peak 1/2. Then the molecule may be reformed by high-temperature gas-phase chemistry in the post-shock gas (Charnley & Kaufman 2000). The primary gas-phase formation route for CO_2 is: $CO + OH \rightarrow CO_2 + H$. This reaction requires a temperature above ~ 100 K. Since CO is abundant throughout the warm gas, the formation of CO_2 is limited by the amount of available OH and it is likely that the OH and CO_2 molecules are co-located. Abundant OH is observed both toward IRc2 and Peak 1 and Peak 2 (Watson et al. 1985; Melnick et al. 1987; Cernicharo et al. 1999), consistent with the widespread CO_2 detection. The OH is produced by high-temperature reactions of O with H_2. However, above $T \sim 230$–300 K all O and OH are driven into H_2O, leaving no OH to form CO_2 (Charnley 1997). This could explain why the rotational excitation temperature toward all three positions does not exceed this value. Since the observed CO_2 abundance toward IRc2/BN is higher than those toward Peak 1 and 2 for scenario 3, this suggests that

reformation of CO_2 must have been taken place here for a longer time than toward Peak 1 and Peak 2. The abundances toward Peak 1 and 2 suggest that reformation has taken place on time scales of $t \lesssim 10^4$ yr for $T \sim 200$ K (Charnley & Kaufman 2000).

If on the other hand, the CO_2 is at most partly destroyed in the shock, then grain-mantle evaporation starts to play a role. In Sect. 3.3 it is shown that grain-mantle evaporation can account for the observed gas-phase CO_2 abundances toward IRc2/BN. Since the temperature of the warm component of the shock is $T \sim 150$–400 K, most of the CO_2 ice will already be evaporated here, and the observed CO_2 ice toward Peak 1 and 2 originates in the extended ridge. This results in CO_2 ice abundances of $N(CO_2)/N(H_2) \sim 6 \times 10^{-7}$ and $\sim 5 \times 10^{-7}$ respectively, as determined from the SWS spectra, using $N(H_2) \sim 3 \times 10^{23}$ cm^{-2} corresponding to the value derived by Sutton et al. (1995) for the extended ridge. Comparison with the CO_2 gas-phase abundances in the case of scenario 3 (Table 3) shows that the ice abundances are much higher than the observed gas-phase CO_2 abundances toward Peak 1 and Peak 2. Assuming that the pre-shock CO_2 ice abundances toward Peak 1 and 2 are similar to those in the extended ridge, this suggests that toward Peak 1 and 2 grain-mantle evaporation probably does not play a dominant role. Thus, the CO_2 gas likely probes the same physical component toward all three positions, but the chemical origin may be different. Toward IRc2 the inferred abundances can be explained by both grain-mantle evaporation and reformation in the gas phase on time scales of $t \sim 10^5$ yr after destruction by the shock or a heating event. The inferred CO_2 abundances toward Peak 1 and 2 are best explained by reformation in the gas phase on time scales $t \lesssim 10^4$ yr after destruction by the shock.

6. Conclusions

1. The HCN ν_2 and C_2H_2 ν_5 ro-vibrational bands have been detected in absorption toward IRc2 and in emission toward Peak 2. The ν_2 ro-vibrational band of CO_2 has been detected in absorption toward IRc2/BN and in emission toward Peak 1 and Peak 2.

2. The observed HCN and C_2H_2 ro-vibrational absorption bands toward IRc2 probably originate in gas that has been blown away from the hot core clumps and now resides in the plateau gas in the cavities between these clumps close to IRc2. Their high abundances can be explained by a combination of high-temperature gas-phase chemistry and grain-mantle evaporation.

3. The CO_2 absorption toward IRc2/BN probably originates in the warm shocked gas (plateau gas) toward both IRc2 and BN, given the similarity of its band shape with the observed emission toward Peak 1 and Peak 2. The inferred CO_2 abundances can be explained by both grain-mantle evaporation and reformation in the gas phase on time scales of $t \sim 10^5$ yr after destruction by the shock or a heating event.

4. The inferred HCN, C_2H_2, and CO_2 abundances from the emission features differ by orders of magnitude, depending on the excitation mechanism. Three different scenarios have been investigated: radiative excitation by the IRc2/BN

complex, collisional excitation only, and excitation by infrared radiation from dust mixed with gas in the warm component of the shock. The latter scenario is preferred.

5. The observed HCN and C_2H_2 band profiles toward Peak 2 suggest an origin either in the extended ridge or the warm component of the shock. In both cases the molecules are probably radiatively excited. In the case of an origin in the warm component of the shock the low HCN and C_2H_2 abundances suggest destruction by the shock or heating on short time scales. When the HCN and C_2H_2 originate in the much cooler extended ridge, the high abundances cannot be explained by current chemical models at $T \sim 50$ K.

6. The CO_2 emission toward Peak 1 and Peak 2 does not show evidence for a hot component at $T \sim 3000$ K and therefore likely originates in gas of $T \sim 150$–200 K, consistent with conditions in the warm component of the shock. The rotational temperature of the CO_2 emission, which is constrained by the observed shape of the Q-branch, shows excellent agreement with the kinetic temperature of the warm H_2 gas toward Peak 2. The CO_2 emission is best explained with radiative excitation by dust mixed with gas within the warm component of the shock at $T \sim 150$–200 K. The inferred CO_2 abundances toward both Peak 1 and Peak 2 can be explained by reformation in the gas phase after destruction in the shock.

7. Further studies of the collisional rate coefficients for vibrational de-excitation of CO_2 with H_2 are needed. Current data suggest that they are at least an order of magnitude higher than those with He, due to vibration-rotation energy transfer.

Appendix A: CO_2 collisional rate coefficients

Little is known about collisional rate coefficients for vibrational excitation, even for the simplest molecules (see discussion in GA02). However, some experimental and theoretical values exist for the vibrational de-excitation rate of the CO_2 $\nu_2 = 1$ to the $\nu_2 = 0$ state by collisions with H_2 and He for temperatures between ~ 150 K and 300 K (Allen et al. 1980; Banks & Clary 1987; Lepoutre et al. 1979). These values are summarized in Fig. A.1. The corresponding excitation rates $k_{0-1}^{CO_2-X}$ can be found by multiplying with the factor $g_{vib} \exp(-E_{vib}/T_k)$, with g_{vib} and E_{vib} the statistical weight and energy of the $\nu_2 = 1$ state, respectively. The collisional de-excitation rates for CO_2–H_2 are at least a factor of 1000 higher than the CO–H_2 rates in the same temperature range (Reid et al. 1997). Since the results of Sect. 4.3 show that the observed CO_2 originates in gas at $T_{ex} \sim 150$–200 K, this suggests that collisions are much more important for CO_2 than for CO.
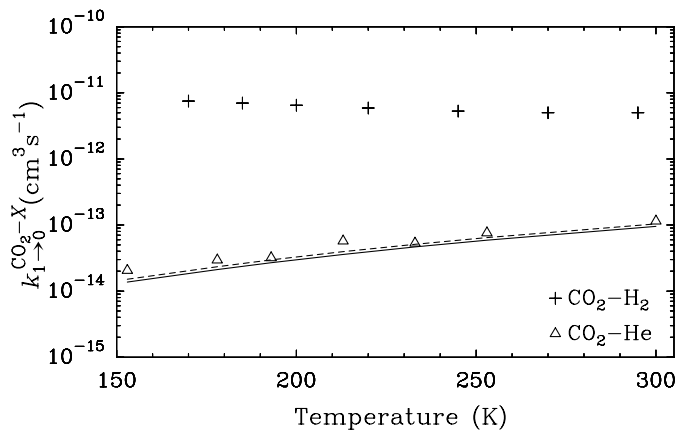
Fig. A.1. Collisional de-excitation rates $k_{1-0}^{CO_2-X}$ for CO_2 from the $v_2 = 1$ to the $v_2 = 0$ state, with collision partner X. Only collisions with H_2 and He are considered. Triangles and plus-signs denote experimental data from Lepoutre et al. (1979) and Allen et al. (1980), respectively. Theoretical calculations for the CO_2-He rates from Banks & Clary (1987) are shown by the thin and dashed lines, showing good agreement with the experimental data.

It should also be noted that the ratio between the CO_2–H_2 and the CO_2–He vibrational de-excitation rates per collision is at least 50 between ~150–300 K (Fig. A.1). This is much higher than the factor of 1.348 based on the difference in reduced mass, which is generally used to convert rotational de-excitation rates of a molecule with He to that with H_2. This may be due to resonances with energy levels in the H_2 molecule (Allen et al. 1980), leading to enhanced vibration-rotation energy transfer and vibrational de-excitation rates for collisions with H_2 compared to those with He. The same large difference is seen between the CO–H_2 and CO–He vibrational de-excitation rates (GA02). Nevertheless, further experimental and theoretical studies of the CO_2–H_2 vibrational de-excitation rates are warranted to confirm the large values adopted here. Since the He abundance is much lower than that of H_2, collisions with He are not important. No data could be found for CO_2–H collisions but assuming that the empirical formula from Millikan & White (1963) used in GA02 is also valid for CO_2–H collisions, we find de-excitation rates a factor of at least ~5 lower than the CO_2–H_2 rates between $T = 150$ K and 300 K. In addition, the abundance ratio H/H_2 is expected to be <1. Together these suggest that collisions with H_2 dominate.

References

Allen, D. C., Scragg, T., & Simpson, C. J. S. M. 1980, Chem. Phys., 51, 279

Banks, A. J., & Clary, D. C. 1987, J. Chem. Phys., 86, 802

Beckwith, S., Persson, S. E., Neugebauer, G., & Becklin, E. E. 1978, ApJ, 223, 464

Bergin, E. A., Goldsmith, P. F., Snell, R. L., & Langer, W. D. 1997, ApJ, 482, 285

Blake, G. A., Sutton, E. C., Masson, C. R., & Phillips, T. G. 1987, ApJ, 315, 621

Blake, G. A., Mundy, L. G., Carlstrom, J. E., et al. 1996, ApJ, 472, L49

Bockelée-Morvan, D., Lis, D. C., Wink, J. E., et al. 2000, A&A, 353, 1101

Boonman, A. M. S., van Dishoeck, E. F., Lahuis, F., Wright, C. M., & Doty, S. D. 2000, in ISO beyond the Peaks, ESA SP-456, 67 [astro-ph/0105249]

Boonman, A. M. S., Stark, R., van der Tak, F. F. S., et al. 2001, ApJ, 553, L63

Boudin, N., Schutte, W. A., & Greenberg, J. M. 1998, 331, 749

Brooke, T. Y., Tokunaga, A. T., Weaver, H. A., et al. 1996, Nature, 383, 606

Carr, J. S., Evans, N. J., II, Lacy, J. H., & Zhou, S. 1995, ApJ, 450, 667

Cernicharo, J., Perez-Martinez, S., González-Alfonso, E., et al. 1999, in The Universe as Seen by ISO, ed. P. Cox, & M. F. Kessler, ESA-SP 427, 651

Charnley, S. B., Tielens, A. G. G. M., & Millar, T. J. 1992, ApJ, 399, L71

Charnley, S. B. 1997, ApJ, 481, 396

Charnley, S. B., & Kaufman, M. J. 2000, ApJ, 529, L111

Chernin, L. M., & Wright, M. C. H. 1996, ApJ, 467, 676

Chernoff, D. F., McKee, C. F., & Hollenbach, D. J. 1982, 259, L97

Dartois, E., D'Hendecourt, L., Boulanger, F., et al. A&A, 331, 651

Doty, S. D., van Dishoeck, E. F., van der Tak, F. F. S., & Boonman, A. M. S. 2002, A&A, 389, 446

Downes, D., Genzel, R., Becklin, E. E., & Wynn-Williams, C. G. 1981, ApJ, 244, 869

Evans, N. J., II, Lacy, J. H., & Carr, J. S. 1991, ApJ, 383, 674

Genzel, R., & Stutzki, J. 1989, ARA&A, 27, 41

Gerakines, P. A., Whittet, D. C. B., Ehrenfreund, P., et al. 1999, ApJ, 522, 357

Gezari, D. Y. 1992, ApJ, 396, L43

Gezari, D. Y., Backman, D. E., & Werner, M. W. 1998, ApJ, 509, 283

González-Alfonso, E., Cernicharo, J., van Dishoeck, E. F., Wright, C. M., & Heras, A. 1998, ApJ, 502, L169

González-Alfonso, E., Wright, C. M., Cernicharo, J., et al. 2002, A&A, 386, 1074 (GA02)

Harwit, M., Neufeld, D. A., Melnick, G. J., & Kaufman, M. J. 1998, ApJ, 497, L105

Helmich, F. P. 1996, Ph.D. Thesis, Leiden Observatory

Hogerheijde, M. R., & van der Tak, F. F. S. 2000, A&A, 362, 697

Kester, D., Beintema, D., & Lutz, D. 2001, in The Calibration Legacy of the ISO Mission, ed. L. Metcalfe, & M. F. K. Kessler, ESA-SP 481, 79

Lacy, J. H., Richter, M. J., Greathouse, T. K., Jaffe, D. T., & Zhu, Q. 2002, PASP, 114, 153

Lahuis, F., Wieprecht, E., Bauer, O. H., et al. 1998, in Astronomical Data Analysis Software and Systems VII, ed. R. Albrecht, R. N. Hook, & H. A. Bushouse, ASP Conf. Ser., 145, 224

Lahuis, F., & van Dishoeck, E. F. 2000, A&A, 355, 699

Lepoutre, F., Louis, G., & Tain, J. 1979, J. Chem. Phys., 70, 2225

Melnick, G. J., Genzel, R., & Lugten, J. B. 1987, ApJ, 321, 530

Millikan, R. C., & White, D. R. 1963, J. Chem. Phys., 39, 3209

Ossenkopf, V., & Henning, Th. 1994, A&A, 291, 943

Reid, J. P., Simpson, C. J. S. M., & Quiney, H. M. 1997, J. Chem. Phys., 106, 4931

Rodgers, S. D., & Charnley, S. B. 2001, ApJ, 546, 324

Rosenthal, D., Bertoldi, F., & Drapatz, S. 2000, A&A, 356, 705

Schilke, P., Walmsley, C. M., Pineau des Forêts, G., et al. 1992, A&A, 256, 595

Schilke, P., Groesbeck, T. D., Blake, G. A., & Phillips, T. G. 1997, ApJS, 108, 301

Schilke, P., Benford, D. J., Hunter, T. R., Lis, D. C., & Phillips, T. G. 2001, ApJS, 132, 281

Stutzki, J., Genzel, R., Harris, A. I., Herman, J., & Jaffe, D. T. 1988, ApJ, 330, L125

Sutton, E. C., Peng, R., Danchi, W. C., et al. 1995, ApJS, 97, 455

van der Tak, F. F. S., van Dishoeck, E. F., Evans, N. J., II, Bakker, E. J., & Blake, G. A. 1999, ApJ, 522, 991

van der Tak, F. F. S., van Dishoeck, E. F., Evans, N. J., II, & Blake, G. A. 2000, ApJ, 537, 283

van Dishoeck, E. F., Helmich, F. P., de Graauw, Th., et al. 1996, A&A, 315, L349

van Dishoeck, E. F. 1998, in Chemistry and Physics of Molecules and Grains in Space, Faraday Discussions, 109, 31

van Dishoeck, E. F., & Blake, G. A. 1998, ARA&A, 36, 317

van Dishoeck, E. F., Wright, C. M., Cernicharo, J., et al. 1998, ApJ, 502, L173

van Dishoeck, E. F., Black, J. H., Boogert, A. C. A., et al. 1999, in The Universe as Seen by ISO, ed. P. Cox, & M. F. Kessler, ESA-SP 427, 437

Watson, D. M., Genzel, R., Townes, C. H., & Storey, J. W. V. 1985, ApJ, 298, 316

Wieprecht, E., Bauer, O. H., Beintema, D. A., et al. 2001, in The Calibration Legacy of the ISO Mission, ed. L. Metcalfe, & M. F. K. Kessler, ESA-SP 481, 54

Wilson, T. L., Serabyn, E., & Henkel, C. 1986, A&A, 167, L17

Wright, C. M. 2000, in Astrochemistry: From Molecular Clouds to Planetary Systems, ed. Y. C. Minh, & E. F. van Dishoeck (San Francisco: Astron. Soc. Pac.), IAU Symp., 197, 177

Wright, C. M., van Dishoeck, E. F., Black, J. H., et al. 2000, A&A, 358, 689

Wright, M. C. H., Plambeck, R. I., & Wilner, D. J. 1996, ApJ, 469, 216

Wynn-Williams, C. G., Genzel, R., Becklin, E. E., & Downes, D. 1984, ApJ, 281, 172

Ziurys, L. M., & Turner, B. E. 1986, ApJ, 300, L19